

Ultrahigh-pressure structural phase transitions in Cr, Mo, and W

John A. Moriarty

Lawrence Livermore National Laboratory, University of California, Livermore, California 94550

(Received 29 July 1991; revised manuscript received 7 October 1991)

On the basis of first-principles total-energy calculations, we predict the ultrahigh-pressure destabilization of the bcc structure in the group-VIB elements Cr, Mo, and W through a bcc→hcp phase transition at pressures of about 7.0, 4.2, and 12.5 Mbar, respectively. In Mo and W, a subsequent hcp→fcc transition is also predicted at about 6.2 and 14.4 Mbar, respectively. The overall driving mechanism for these transitions is a continuous $sp \rightarrow d$ transfer of electrons upon compression, although other factors play an important quantitative role, especially the hard-core-like interaction between the large cores of these elements, which disfavors the bcc structure and serves to lower the bcc→hcp transition pressures. While the actual predicted transition pressures are sensitive to the details of the calculations, the qualitative trends are not, and the bcc→hcp transition in Mo should be within reach of static diamond-anvil-cell experiments. In this regard, we have also calculated accurate 300-K isotherms for bcc Cr, Mo, and W valid up to the 5–6-Mbar pressure range.

I. INTRODUCTION

Structural phase stability in transition and rare-earth metals is controlled to a large extent by the number of valence d electrons per atom, Z_d . Simple rigid-band models^{1,2} with Z_d as the single variable parameter can explain most of the observed trends, and these models, in turn, are well supported by first-principles quantum-mechanical calculations.³ The rare earths have been the most systematically studied of the two groups of elements regarding trends with both atomic number and pressure. In these metals, Z_d is found to increase both with decreasing atomic number through the series and with increased pressure for a given element, such that, for either variation, the same sequence of structures is predicted, in agreement with experiment.⁴ In transition metals, on the other hand, Z_d is increased by increasing atomic number, and, except for the late members of each series, also by the application of high pressure. The variation of Z_d with atomic number explains the canonical hcp-bcc-hcp-fcc sequence of structures observed across the nonmagnetic $4d$ and $5d$ transition series and is responsible for the extreme stability of the bcc structure in the group-VIB elements Mo and W compared with the stable hcp structure of the corresponding group-VIIB elements Tc and Re. The general increase in Z_d with pressure shared in common between the rare-earth and transition metals results from an $sp \rightarrow d$ transfer of valence electrons under compression. This so-called $s \rightarrow d$ transition⁵ arises from the fact that the spatially extended s and p states feel the effects of high pressure more strongly than do the localized d states. Thus, the corresponding s and p energy bands rise in energy faster than do the d bands, transferring electrons from s - and p -like states to d -like states in the process.

Unlike the rare earths, the central transition metals are relatively incompressible in nature, making their phase diagrams difficult to study at the multimegabar pressures

needed to induce phase changes in these materials. Although there has been long-standing speculation on a possible high-pressure bcc→hcp transition in Mo based on empirical alloy data,⁶ this question has only recently been investigated, where, in collaboration with other workers, we produced direct experimental and theoretical evidence for such a phase transition.⁷ The experimental evidence consisted of acoustic-velocity data obtained along the shock Hugoniot which showed a sharp break at about 2.1 Mbar (and ≈ 4000 K). This is indicative of a solid-solid phase transition and occurs well prior to melting, which was detected at about 3.9 Mbar in the same series of experiments. These experiments do not, however, provide any information about the structure of the final phase of the solid-solid transition. The corresponding theoretical evidence was in the form of preliminary first-principles total-energy calculations, based on the linear-muffin-tin-orbital (LMTO) method, which predicted a zero-temperature bcc→hcp transition near 3.2 Mbar in the nonrelativistic limit. The purpose of the present paper is to follow up on the theoretical aspects of this work with a more in-depth analysis on the low-temperature energetics of the group-VIB metals. This includes refined relativistic LMTO calculations on Mo, which raise the predicted zero-temperature bcc→hcp transition pressure to above 4 Mbar, and LMTO calculations on the other group-VIB elements Cr and W. Other workers are actively pursuing additional ultrahigh-pressure experiments on these metals. Preliminary acoustic-velocity measurements have now been made on W, revealing an analogous solid-solid phase transition at about 4.3 Mbar.⁸ Diamond-anvil-cell experiments on Mo and W at multimegabar pressures are also in progress.^{9,10} In these experiments, Mo has already been taken above 4 Mbar, but with no evidence yet of a phase transition.¹⁰

II. ELEMENTARY STRUCTURAL PREDICTIONS

Before proceeding with the full theoretical analysis, it is instructive to consider some of the immediate implica-

tions for high-pressure phase stability in the central transition metals based on the aforementioned rigid-band model for the electronic structure with variable Z_d . These implications can be inferred from Fig. 1, where we have schematically plotted the bcc-fcc and hcp-fcc energy differences as a function of Z_d one would obtain from such a model for the nonmagnetic 3d, 4d, and 5d series at ambient conditions. If there exists positive $sp \rightarrow d$ electron transfer with compression, which is true at least through the group-VIIB metals (Mn, Tc, and Re), then increasing pressure for a given element corresponds structurally to moving to the right in Fig. 1. As a practical matter sp - d electron transfer can only induce changes $\Delta Z_d < 1$ under compression, so that the structural consequences of high pressure for most of the central transition metals can be inferred by examining the elemental group just to the right of the one under consideration. For example, if the group to the right has the same crystal structure, then no high-pressure phase transitions are expected. From Fig. 1, one thus predicts that the group-VB elements (V, Nb, and Ta) should remain bcc under high pressure since their neighbors to the right (Cr, Mo, and W) are also bcc. Experimentally, shock-compressed Ta, unlike Mo and W, shows no break in its acoustic velocity prior to melting at about 3 Mbar,¹¹ suggesting that, indeed, no solid-solid transition has occurred. Similarly, one expects the group-VIIB metals [Mn (nonmagnetic), Tc, and Re] to remain stable in the hcp structure. Within this group, Re has been studied in the diamond-

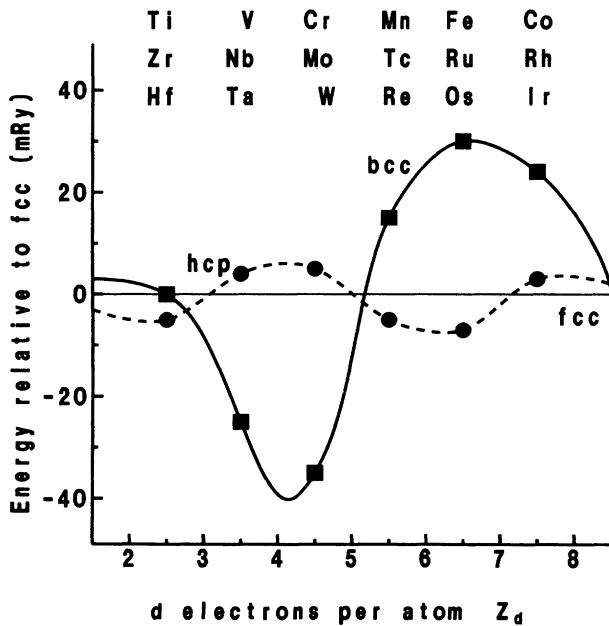


FIG. 1. Schematic representation of bcc-fcc and hcp-fcc energy differences as a function of d -band occupation for the nonmagnetic 3d, 4d, and 5d transition-metal series at ambient conditions. Equating positive pressure with increasing Z_d permits elementary predictions about the high-pressure phase stability of each group of elements, as discussed in the text.

anvil cell to 2.16 Mbar with no evidence of a structural change.¹² Furthermore, corresponding theoretical total-energy calculations show that the hcp structure becomes slightly more stable with respect to bcc (the structure of the group-VIB elements to the left) under compression.¹³ This is consistent with a gradual $s \rightarrow d$ transition and positive ΔZ_d under high pressure.

For the remaining elemental groups shown in Fig. 1, on the other hand, high-pressure structural phase transitions are suggested. In the group-IVB metals (Ti, Zr, and Hf), for example, one immediately predicts an hcp \rightarrow bcc transition. In this case, there is known to be an intermediate ω phase, which is a hexagonal distortion of bcc, so that the actual sequence is hcp $\rightarrow \omega \rightarrow$ bcc. This full sequence has recently been demonstrated for both Zr and Hf in diamond-anvil-cell experiments,^{14,15} as well as in theoretical total-energy calculations.¹⁶ Moreover, in the case of Hf, the final bcc structure has been shown to have a wide stability range, from 0.71 to at least 2.52 Mbar,¹⁵ suggesting that bcc is indeed the ultimate phase as predicted from Fig. 1. In the group-VIB metals (Cr, Mo, and W), which is the central focus of the present paper, the elementary prediction is for the complementary bcc \rightarrow hcp transition. As we shall demonstrate in Sec. III, this prediction is indeed consistent with full first-principles calculations. Finally, in the group-VIII elements there is the possibility of a hcp \rightarrow fcc transition for the Fe-group elements [Fe (nonmagnetic), Ru, and Os] if there remains positive $sp \rightarrow d$ electron transfer under high pressure. However, diamond-anvil-cell measurements on ϵ -Fe indicate that the high-pressure hcp phase remains stable to at least 3 Mbar.¹⁷ Perhaps more likely is the reverse fcc \rightarrow hcp transition in the Co-group elements [Co (nonmagnetic), Rh, and Ir], which could occur if the normal $sp \rightarrow d$ electron transfer has been reversed into a $d \rightarrow sp$ transfer due to competing sp - d hybridization effects. This possibility remains to be investigated, although the existence of reverse $d \rightarrow sp$ electron transfer has been theoretically established in two other fcc transition metals to the right of the Co group, namely, Cu (Ref. 18) and Pt.¹⁹

III. FIRST-PRINCIPLES STRUCTURAL CALCULATIONS

The high-pressure electronic structure and energetics of Cr, Mo, and W have been studied theoretically within the framework of the Kohn-Sham local-density formalism,²⁰ utilizing the first-principles linear-muffin-tin-orbital band-structure method^{21,22} together with Hedin-Lundqvist exchange and correlation.²³ All of the present self-consistent LMTO calculations have employed the atomic-sphere approximation (ASA), the combined-correction term to this approximation,^{21,22} and s , p , d , and f angular momentum components. Because the LMTO-ASA approach is best suited to highly symmetric and relatively close-packed structures, we have confined our attention in the present study to bcc, fcc, and ideal hcp crystal lattices at zero temperature. Our analysis of phase stability in the group-VIB metals is based on calculations of the total energy of each solid (excluding zero-

point vibrational contributions) as a function of atomic volume Ω and crystal structure over a wide volume range, typically $0.4 \leq \Omega/\Omega_0 \leq 1.1$, where Ω_0 is the equilibrium volume. As has been well established for simple metals,²⁴ total-energy differences between relatively close-packed structures in transition metals at fixed volume are almost identical to Gibbs free-energy differences at fixed pressure, so we have focused on only the former. Corresponding pressure-volume relations have been calculated for the bcc and fcc structures of each metal and used to translate the average phase-transition volumes so obtained to transition pressures. These relations have also been used to calculate room-temperature isotherms for bcc Cr, Mo, and W, as discussed in Sec. IV.

In the present LMTO calculations, the $3d$ metal Cr has been treated in a nonrelativistic mode, while the $5d$ metal W has been treated in a semi- or scalar-relativistic mode in which all relativistic corrections except spin orbit are included. For the intermediate $4d$ metal Mo, we have done parallel nonrelativistic and scalar-relativistic calculations. While relativistic corrections in Mo are generally small, we have found that they do have a significant impact on the predicted transition pressures, as will be discussed below. In all cases both the core and valence electrons have been treated self-consistently. Full energy bands have been calculated for the valence states and for the large outer-core states ($3s$ and $3p$ in Cr; $4s$ and $4p$ in Mo; $5s$, $5p$, and $4f$ in W), while an atomic treatment has been used for the remaining inner-core states. The broad valence bands have been sampled with a high number of \mathbf{k} points in the Brillouin zone (BZ), while the narrow outer-core bands have been sampled with a lesser fixed number of points. In our structural calculations, the number of valence-band points was increased until little or no further difference in bcc-fcc and hcp-fcc energy differences was found, and the results reported below are based on 506, 505, and 252 \mathbf{k} points in the irreducible BZ wedges for the bcc, fcc, and hcp structures, respectively. The preliminary structural results on Mo presented in Ref. 7, on the other hand, were based on a nonrelativistic treatment with 285, 240, and 150 \mathbf{k} points.

In the LMTO-ASA method, each Wigner-Seitz polyhedron is approximated by an atomic sphere of radius R_{WS} in which the electron density $n(r)$ is spherically averaged. The corresponding one-electron potential $V(r)$ for an elemental metal of atomic number Z_a is then given by

$$V(r) = -\frac{Z_a e^2}{r} + v(r) + v_{\text{xc}}(r), \quad (1)$$

where $v(r)$ and $v_{\text{xc}}(r)$ are the Coulomb potential and the local exchange-correlation potential, respectively, arising from $n(r)$. In the present work, the total energy per atom, E_{tot} , has been evaluated in the form

$$E_{\text{tot}} = \frac{1}{N} \sum_{\alpha} E_{\alpha} - \int_0^{R_{\text{WS}}} 4\pi r^2 n(r) \left[\frac{1}{2} v(r) + v_{\text{xc}}(r) - \varepsilon_{\text{xc}}(r) \right] dr + E_{\text{es}}. \quad (2)$$

The first term in Eq. (2) is the usual sum over occupied one-electron eigenvalues and includes both the valence and outer-core energy bands, $E_{\alpha} = E(\mathbf{k})$, and the discrete inner-core levels. The second term represents the double-counting and exchange-correlation corrections of the local-density formalism evaluated within the ASA. The third and final term in Eq. (2) is an additional electrostatic correction, which has variously been called the muffin-tin, Ewald, or Madelung correction in the LMTO literature, and is given by

$$E_{\text{es}} = \frac{1}{2} [n(R_{\text{WS}})\Omega e]^2 \frac{1.8 - \alpha_E}{R_{\text{WS}}}, \quad (3)$$

where α_E is the familiar electrostatic Ewald (or Madelung) constant of the lattice in question ($\alpha_E = 1.79186$ for bcc, 1.79175 for fcc, and 1.79168 for ideal hcp). This latter term is retained here as a desirable improvement over the strict ASA for both the structural-energy differences and the pressure-volume relations, although its quantitative impact on the present results is typically small. Pressures can be obtained either by differentiating Eq. (2) with respect to volume or using the equivalent Pettifor-Liberman surface integral expression²⁵ for the contribution of the first two terms. The latter approach has been used in the present work.

Within the LMTO-ASA framework, structural energies may be obtained in several different ways. To determine the best approach for the present intended applications, we have investigated this question in considerable detail for the case of nonrelativistic Mo. Three methods have been tried: (i) direct total-energy subtraction, (ii) valence binding-energy subtraction, and (iii) the so-called Andersen force theorem.²⁶ In the total-energy subtraction method, a full self-consistent calculation for each volume and structure of interest is required and one calculates the total-energy difference between two structures, ΔE_{tot} , directly from Eq. (2). This method suffers from the obvious problem of having to include extremely large, but structurally irrelevant, inner-core energy contributions in E_{tot} . In the absence of ultrahigh levels of convergence, such inner-core energies can give rise to small but damaging amounts of numerical noise. In the present study, we have been able to obtain satisfactory bcc-fcc total-energy differences, since these are relatively large and require convergence of ΔE_{tot} to only about ± 1 mRy. Satisfactory hcp-fcc differences, however, which require convergence to about ± 0.1 mRy, could not be obtained. Method (ii), based on valence binding-energy subtraction, readily solves this problem. This method has been adapted from our work on the complementary generalized pseudopotential theory (GPT) of transition metals¹⁸ and has not previously been applied in the context of LMTO-ASA calculations. The basic idea is to separate E_{tot} into valence, core, and valency-core overlap contributions:

$$E_{\text{tot}} = E_{\text{bind}} + E_{\text{core}} + \delta E_{\text{val-core}}. \quad (4)$$

The valence binding energy E_{bind} is that associated with all states treated as energy bands and the core energy E_{core} that associated with the remaining inner-core states.

The residual valency-core overlap energy $\delta E_{\text{val-core}}$ arises from the nonlinear dependence of v_{xc} and ϵ_{xc} on the electron density n . This term is consequently restricted to only exchange-correlation contributions from the inner-core regions of space where valence and core wave functions overlap. One then assumes that E_{core} and $\delta E_{\text{val-core}}$ are independent of structure, so that

$$\Delta E_{\text{tot}} = \Delta E_{\text{bind}} . \quad (5)$$

This method immediately eliminates the core-noise problem of method (i) and, in our test study on Mo, readily produced satisfactory bcc-fcc and hcp-fcc energy differences, with a typical convergence level of ± 0.1 mRy. Method (iii), based on the Andersen force theorem, goes one step further by effectively developing ΔE_{tot} as an expansion in δn , the difference in electron density between the two structures in question. One thereby obtains to first order in δn the simplified result

$$\Delta E_{\text{tot}} = \Delta \left[\sum_{\mathbf{k}} E(\mathbf{k}) \right] + \Delta E_{\text{es}} . \quad (6)$$

In this expression the sum over inner-core energy levels as well as the double-counting and exchange-correlation corrections of Eq. (2) have dropped out. Moreover, the band-structure contribution to Eq. (6) refers to a restricted variation in which $E(\mathbf{k})$ is calculated for the two structures in question with the same atomic-sphere potential $V(r)$. In all our applications of this result, $V(r)$ has been chosen to be the self-consistent potential for the fcc structure. In our test study on Mo, Eq. (6) produced bcc-fcc and hcp-fcc energy differences as a function of volume which were in close agreement with those obtained from Eq. (5), so we regard methods (ii) and (iii) as

TABLE I. Calculated bcc-fcc and hcp-fcc structural energy differences for the group-VIB metals at equilibrium ($\Omega = \Omega_0$). Theoretical treatments are nonrelativistic (nonrel.) or scalar relativistic (rel.), as indicated. All energies in mRy.

| | Present ^a | Skriver ^b | Mattheiss ^c | Chan ^d |
|--------------|----------------------|----------------------|------------------------|-------------------|
| Cr (nonrel): | | | | |
| bcc-fcc | -28.9 | -28.9 ^e | -29.6 ^e | |
| hcp-fcc | 3.3 | 3.8 ^e | | |
| Mo (nonrel): | | | | |
| bcc-fcc | -30.0 | | | -29.9 |
| hcp-fcc | 2.0 | | | 0.5 |
| Mo (rel): | | | | |
| bcc-fcc | -31.8 | -34.0 | -32.8 | |
| hcp-fcc | 2.7 | 2.6 | | |
| W (rel): | | | | |
| bcc-fcc | -38.3 | -38.8 | -37.1 | -40.3 |
| hcp-fcc | 4.8 | 5.0 | | 3.9 |

^aLMTO-ASA using Eq. (6), with band treatment of outer core and ΔE_{es} correction included via Eq. (3).

^bLMTO-ASA from Ref. 3, with atomic treatment of outer core and $\Delta E_{\text{es}} = 0$.

^cLinear-augmented-plane-wave method from Ref. 27, with atomic treatment of outer core.

^d*Ab initio* pseudopotential method from Ref. 28.

^eScalar relativistic.

essentially equivalent for structural calculations on the group-VIB metals. The principal advantage of the Andersen force-theorem method (iii) is that only one fully self-consistent calculation per volume is required. For this reason, the remainder of our structural calculations on Cr, Mo, and W have been carried out using this method.

At equilibrium ($\Omega = \Omega_0$), there have been several previous calculations of bcc-fcc and hcp-fcc structural energy differences for the group-VIB metals using local-density band-structure methods.^{3,27,28} In Table I we compare these results with our present values for Cr, Mo, and W obtained via Eq. (6). There is seen to be good overall agreement. In each case the observed bcc structure is stabilized with a large negative bcc-fcc energy difference, which increases in magnitude from Cr to Mo to W, and a small positive hcp-fcc energy difference, which is smallest for Mo and largest for W. The small quantitative differences seen in Table I are attributable to secondary approximations, either inherent in the various methods or made by physical choice.

Our corresponding LMTO-ASA calculations of bcc-fcc and hcp-fcc energy differences for the group-VIB metals as a function of volume are presented in Figs. 2–4 for Cr, (relativistic) Mo, and W, respectively. (The result for nonrelativistic Mo is analogous to the relativistic case and is not shown.) The behavior of the large bcc-fcc energy difference with decreasing volume is quite similar in all three metals. This quantity decreases slowly to a minimum value and then increases rapidly and dramatically over a relatively narrow volume range, becoming large and positive beyond twofold compression and thus ensuring the ultrahigh-pressure destabilization of the bcc structure. The behavior of the smaller hcp-fcc energy difference with decreasing volume, on the other hand,

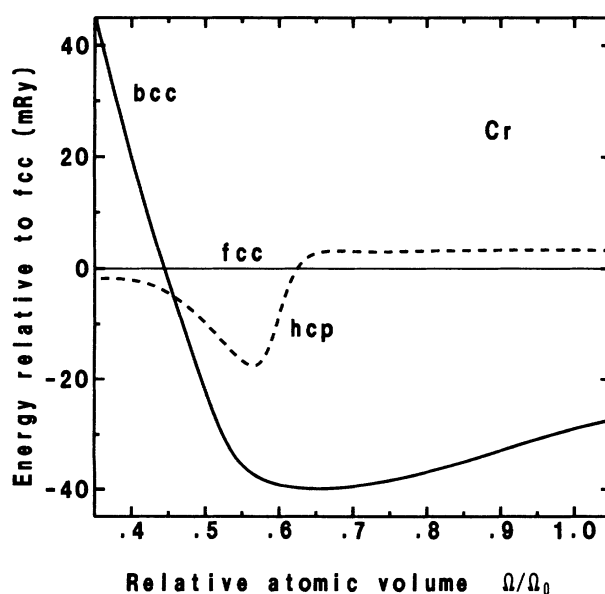


FIG. 2. Present theoretical bcc-fcc and hcp-fcc total-energy differences for Cr as a function of volume.

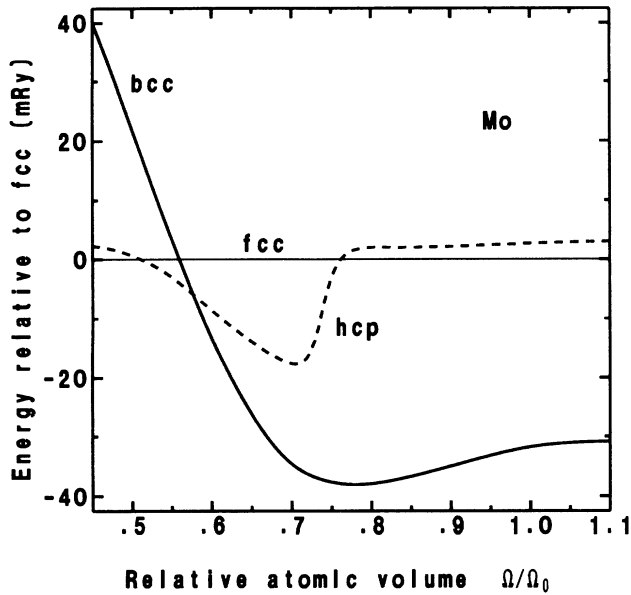


FIG. 3. Present theoretical bcc-fcc and hcp-fcc total-energy differences for Mo as a function of volume from the scalar-relativistic treatment.

shows some subtle variation from metal to metal. In Cr and Mo, this quantity initially stays rather constant at a small positive value before dropping rapidly to a negative minimum. It then rises again towards zero, crossing the bcc-fcc curve in the process and thereby indicating a bcc→hcp transition. In Cr, the hcp-fcc difference remains negative at the smallest volume considered, while in Mo it returns to a positive value indicating a subsequently hcp→fcc transition. In W, the hcp-fcc energy

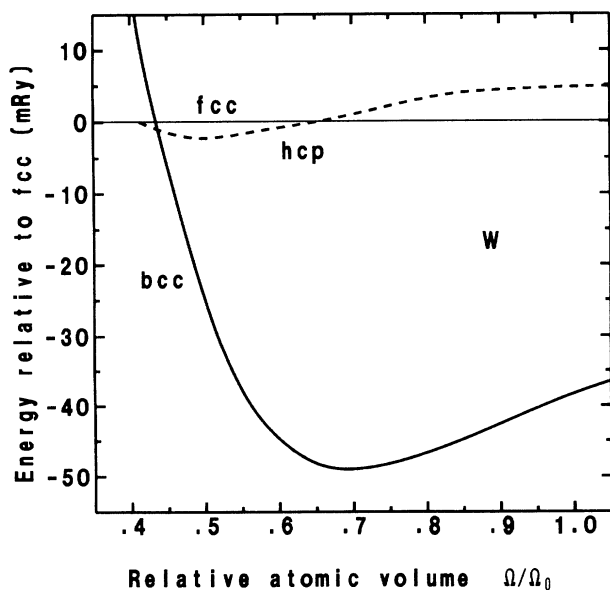


FIG. 4. Present theoretical bcc-fcc and hcp-fcc total-energy differences for W as a function of volume.

TABLE II. Predicted average transition volumes (Ω/Ω_0) and pressures (P) for Cr, Mo, and W from the present theoretical calculations. Treatments are nonrelativistic (nonrel.) or scalar relativistic (rel.), as indicated. Here $\Omega_0=80.94$ for Cr, 105.1 for Mo, and 107.0 for W, with all values in a.u. Pressures are given in Mbar.

| Treatment | bcc→hcp | | hcp→fcc | |
|-------------|-------------------|------|-------------------|------|
| | Ω/Ω_0 | P | Ω/Ω_0 | P |
| Cr: nonrel. | 0.470 | 7.0 | | |
| Mo: nonrel. | 0.625 | 3.1 | 0.565 | 4.5 |
| rel. | 0.580 | 4.2 | 0.515 | 6.2 |
| W: rel. | 0.440 | 12.5 | 0.420 | 14.4 |

difference displays a more symmetric oscillation about zero with decreasing volume, returning to a slightly positive value at the smallest volume considered with both bcc→hcp and hcp→fcc transitions predicted. Average transition volumes obtained from these total-energy calculations together with the corresponding transition pressures are given in Table II. In these results the transition volumes have been determined graphically to an estimated accuracy of ± 0.005 in Ω/Ω_0 . All of the predicted phase transitions occur in the vicinity of twofold compression with the transition volumes in the range $0.420 \leq \Omega/\Omega_0 \leq 0.625$. In this regime, pressure is increasing rapidly with decreasing volume, so that the pre-

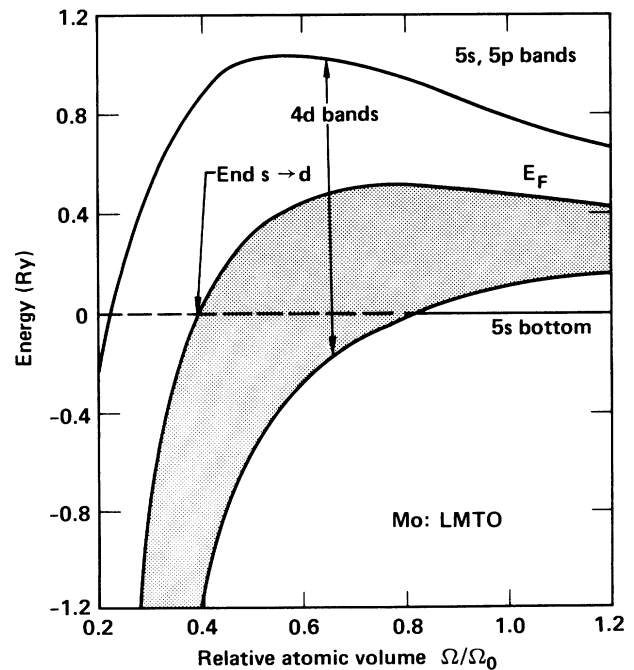


FIG. 5. Lowering of the 4d bands and the Fermi level E_F relative to the 5s and 5p bands with decreasing volume for nonrelativistic Mo. Nominal end to the $s \rightarrow d$ transition occurs when E_F falls below the bottom of the 5s band. Included in the calculation but not shown are the complicating effects of $sp-d$ hybridization and the emergence of the outer-core 4s and 4p bands from below. Occupied portion of the 4d bands is shaded.

dicted transition pressures are sensitive to the calculational details. The general trends, however, seem to be clearly established and, in particular, note that the lowest transition pressures are predicted for the $4d$ element Mo and the highest for the $5d$ element W. This unusual ordering is similar to what occurs in the group-IVB metals,¹⁴⁻¹⁶ where the $4d$ element Zr has the lowest transition pressures for both the $\text{hcp} \rightarrow \omega$ and $\omega \rightarrow \text{bcc}$ transitions.

As suggested in Sec. II, the overall driving mechanism for the present phase transitions is an $sp \rightarrow d$ transfer of electrons with compression. The importance of this mechanism in the group-VIB metals can be immediately appreciated from Fig. 5, where we have plotted the relative movement under high pressure of the $4d$ valence energy bands and Fermi level E_F with respect to the bottom of the $5s$ band for the case of (nonrelativistic) Mo. This plot illustrates the dramatic lowering of these d bands below the valence s and p bands with decreasing volume. In the context of the LMTO-ASA method, the corresponding variation in the band-electron populations may be monitored by integrating the angular momentum components of the valence electron density. Specifically, we define Z_d to be the integrated $l=2$ component of this density. While the additional competing effects of $sp-d$ hybridization and the emergence of the outer-core energy bands from below combine to limit the amount of electron transfer, ΔZ_d , which can actually occur at high pressure, in the volume regime of the present phase transitions Z_d is indeed found to be monotonically increasing with decreasing volume for a given crystal structure. This is shown in Figs. 6-8 for Cr, (relativistic) Mo, and W, respectively. Here we have plotted $Z_d(\Omega)$ for the bcc

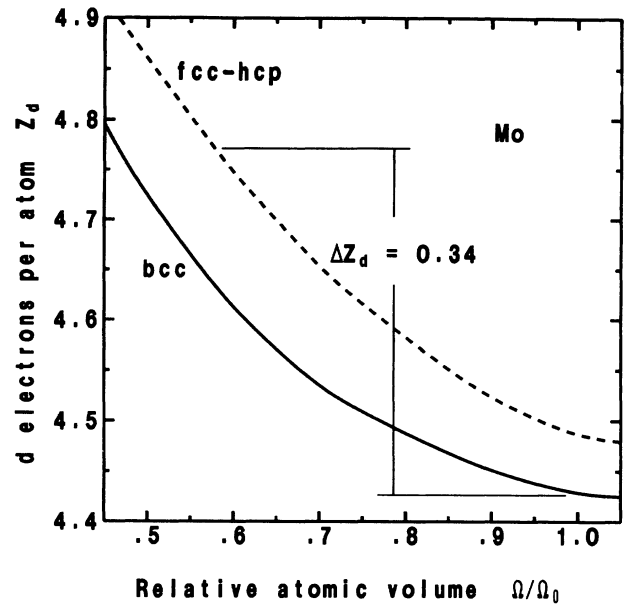


FIG. 7. Calculated d -band occupation for bcc and fcc (or hcp) Mo as a function of volume from the scalar-relativistic treatment. The quantity $\Delta Z_d = 0.34$ is the net increase between equilibrium ($\Omega = \Omega_0$) and the end of the $\text{bcc} \rightarrow \text{hcp}$ transition ($\Omega = 0.58\Omega_0$).

and fcc structures in each case, noting that the result for the hcp structure is almost the same as for fcc. We have also indicated in each plot the net amount of electron transfer ΔZ_d which corresponds to the $\text{bcc} \rightarrow \text{hcp}$ transition. These amounts are 0.43, 0.34, and 0.50

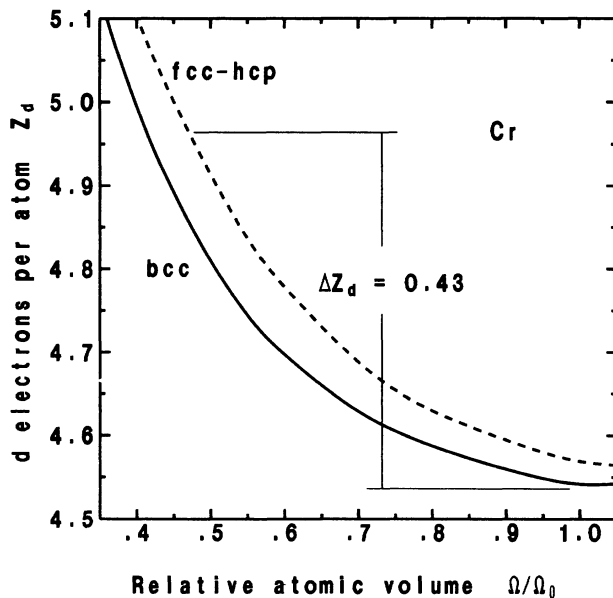


FIG. 6. Calculated d -band occupation for bcc and fcc (or hcp) Cr as a function of volume. The quantity $\Delta Z_d = 0.43$ is the net increase between equilibrium ($\Omega = \Omega_0$) and the end of the $\text{bcc} \rightarrow \text{hcp}$ transition ($\Omega = 0.47\Omega_0$).

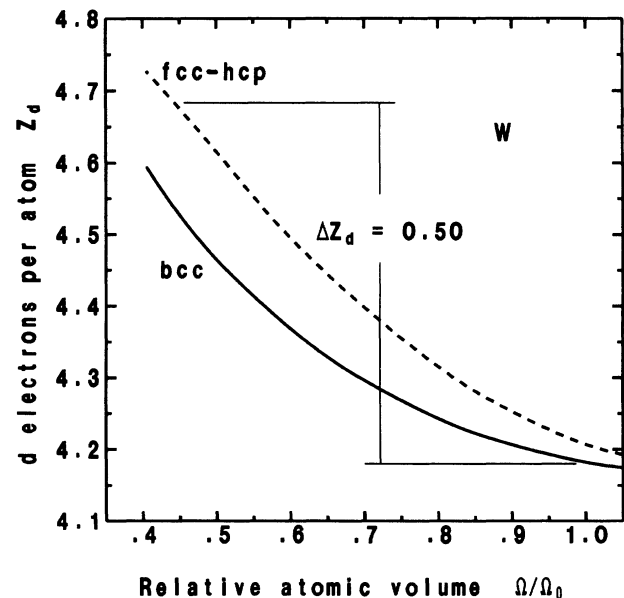


FIG. 8. Calculated d -band occupation for bcc and fcc (or hcp) W as a function of volume. The quantity $\Delta Z_d = 0.50$ is the net increase between equilibrium ($\Omega = \Omega_0$) and the end of the $\text{bcc} \rightarrow \text{hcp}$ transition ($\Omega = 0.44\Omega_0$).

electrons/atom for Cr, Mo, and W, respectively, and correlate with the calculated transition pressures of 7.0, 4.2, and 12.5 Mbar. These results are also in accord with one's expectation from Fig. 1 that roughly one-half an electron per atom must be transferred to drive the bcc \rightarrow hcp transition.

In addition to the overall influence of $sp\rightarrow d$ electron transfer on phase stability, other factors appear to be important here in raising or lowering the transition pressures for an individual element. In particular, the large ion cores in the group-VIB metals lead to a repulsive hard-core-like interaction between near neighbors under high pressure. As is well known, hard-core repulsing disfavors the bcc structure with respect to the more close-packed fcc and hcp structures because of the shorter bcc nearest-neighbor distance. In the present context, such an interaction thus serves to lower the bcc \rightarrow hcp transition pressure. We believe that this effect is at least partially responsible for the relatively low-transition pressures we find in Mo, since the repulsive core interaction enters sooner as a function of compression in this metal than in either Cr or W. This is demonstrated in Fig. 9, where we have plotted the core component of the total pressure for the group-VIB metals as a function of Ω/Ω_0 in the vicinity of our predicted transitions. The core pressure is clearly seen to be largest in Mo and smallest in W, in exact inverse order to the calculated bcc \rightarrow hcp transition pressures. Figure 9 also helps to explain the sensitivity of our calculated transition pressures in Mo to relativistic effects, as displayed in Table II. One expects relativistic effects to shrink the size of the ion core and thus reduce direct core interactions, so that the core pressure is lowered and the bcc \rightarrow hcp transition pressure is raised. As demonstrated in Fig. 9 and Table II, this is indeed what happens in our calculations.

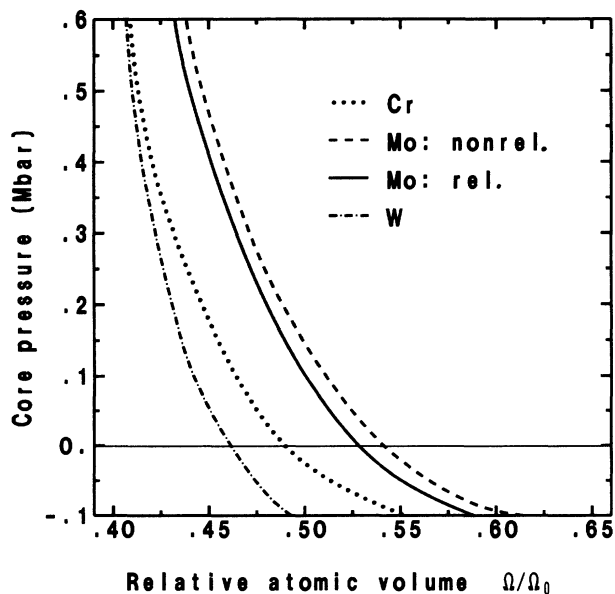


FIG. 9. Calculated core pressures for Cr, Mo, and W in the vicinity of the present bcc \rightarrow hcp and hcp \rightarrow fcc phase transitions.

IV. EQUATION OF STATE

The pressure-volume relations developed in connection with our structural studies have also been applied to the calculation of reliable 300-K isotherms for bcc Cr, Mo, and W up to the 5–6-Mbar pressure range. As in the structural calculations, the question of the equation of state for the group-VIB elements has been considered most extensively in the case of nonrelativistic Mo. In general, total energies and pressures in metals at finite temperature may be calculated as a sum of zero-temperature, ion-thermal, and electron-thermal contributions.^{29,30} Thus, for the total pressure at volume Ω and temperature T , one has

$$P(\Omega, T) = P_0(\Omega) + P_{\text{ion}}(\Omega, T) + P_{\text{el}}(\Omega, T). \quad (7)$$

In this expression the zero-temperature pressure P_0 is immediately available to us from our LMTO results, as is the electron-thermal pressure P_{el} for $k_B T/E_F \ll 1$, which may be obtained from the standard low-temperature expansion of the band-structure energy involving the density of electronic states at the Fermi level E_F . The additional ion-thermal pressure P_{ion} , however, requires a separate treatment of phonons in the solid and, above the melting temperature, itinerant ion motion in the liquid. This is complicated in the central transition metals because of the need to take into account both central and angular forces, but can be addressed by means of generalized pseudopotential theory. The GPT method provides transferable interatomic potentials and forces within the local-density framework which can be used to calculate phonons from quasiharmonic lattice dynamics and, more generally, to perform molecular-dynamics simulations of the high-temperature solid and the liquid. In the case of nonrelativistic Mo, the GPT has been applied in detail to obtain ion-thermal energies and pressures via quasiharmonic lattice dynamics, and then a complete equation of state for the solid has been constructed by means of Eq. (7).^{30,31} The principal Hugoniot for Mo has been calculated with this equation of state and found to be in good agreement with experiment up to the maximum pressure considered (≈ 4 Mbar).³⁰

Our present goal is more modest than the full equation of state and accordingly a more approximate procedure has been developed to obtain the 300-K isotherm at high pressure. In this regard, it has been first noted that, within quasiharmonic lattice dynamics, the high-temperature ion-thermal pressure becomes

$$P_{\text{ion}}(\Omega, T) = P_{\text{zero}}(\Omega) + 3\gamma_{\text{ion}}(\Omega)k_B T/\Omega, \quad (8)$$

where P_{zero} is the small zero-point vibrational contribution to the pressure and γ_{ion} is the familiar ion-Grüneisen parameter. Detailed GPT studies on nonrelativistic Mo (Ref. 31) have shown that $P_{\text{zero}}(\Omega)$ and $\gamma_{\text{ion}}(\Omega)/\Omega$ are rather slowly varying functions of volume for a given crystal structure. Therefore, along the 300-K bcc isotherm, it is reasonable to take $P_{\text{ion}} \approx \text{const}$ and $P_{\text{el}} = 0$, since $P_{\text{ion}} \gg P_{\text{el}}$ and at high pressure $P_0 \gg P_{\text{ion}}$. In addition, it is convenient to normalize $P(\Omega, 300)$ to experiment by requiring that $P(\Omega_0, 300) = 0$, where Ω_0 is the

TABLE III. Cohesive properties of bcc Cr, Mo, and W from the present theoretical calculations. Treatments are nonrelativistic (nonrel.) or scalar relativistic (rel.), as indicated. The calculated equilibrium volume Ω_{eq} has been obtained from the condition $P_0(\Omega_{\text{eq}})=0$. The values of the bulk modulus B_0 and its first pressure derivative B'_0 are those obtained from universal equation-of-state fits to the calculated pressure-volume relations, as discussed in the text, with B_0 and B'_0 evaluated at the experimental equilibrium volume (Ω_0). Units: Ω_{eq} in a.u.; P_0 and B_0 in Mbar.

| | Treatment | Ω_{eq} | $P_0(\Omega_0)$ | B_0 | B'_0 |
|-----|-----------|----------------------|-----------------|-------------------|-------------------|
| Cr: | nonrel. | 74.21 | -0.172 | 2.07 | 4.53 |
| | expt. | 80.94 ^a | 0.0 | 1.98 ^b | |
| Mo: | nonrel. | 105.2 | 0.002 | 2.65 | 4.38 |
| | rel. | 103.2 | -0.045 | 2.48 | 4.99 |
| | expt. | 105.1 ^a | 0.0 | 2.63 ^c | 4.44 ^c |
| W: | rel. | 105.3 | -0.047 | 2.99 | 4.51 |
| | expt. | 107.0 ^a | 0.0 | 3.11 ^c | 4.29 ^c |

^aRoom-temperature value from Ref. 32.

^bRoom-temperature value quoted from Table 1 of Ref. 35.

^cRoom-temperature value from Ref. 36.

observed room-temperature equilibrium volume.³² These three conditions are met by calculating the 300-K isotherm as simply

$$P_{300}(\Omega) \equiv P(\Omega, 300) = P_0(\Omega) - P_0(\Omega_0), \quad (9)$$

which amounts to a rigid shift of the zero-temperature result by an amount $-P_0(\Omega_0)$. At the high pressures of interest here, this procedure is adequate as long as $|P_0(\Omega_0)|$ is a small constant (of roughly the same order as P_{ion}), so that $P_0(\Omega)$ alone yields a good estimate of the equilibrium volume. As shown in Table III, this is indeed the case for the group-VIB metals, especially for Mo and W where $|P_0(\Omega_0)| < 50$ kbar. By comparison, we calculate $P_{\text{ion}}(\Omega_0, 300) = 18$ kbar for nonrelativistic Mo.

For expected further applications, the 300-K isotherms so obtained have been fit with the modified universal equation-of-state form^{33,34}

$$P_{300}(X) = P_T [(1-X)/X^2] \exp[\eta(1-X) + \beta(1-X)^2], \quad (10)$$

TABLE IV. Universal equation-of-state parameters (P_T , η , and β) obtained from fits to the present theoretical 300-K isotherms for bcc Cr, Mo, and W, as described in the text. Theoretical treatments are nonrelativistic (nonrel.) or scalar relativistic (rel.), as indicated. The quantity P_{max} is the upper pressure limit for each fit, with P_T and P_{max} in Mbar.

| | Treatment | P_T | η | β | P_{max} |
|-----|-----------|--------|--------|---------|------------------|
| Cr: | nonrel. | 6.2233 | 5.3012 | 0.0 | 6.0 |
| Mo: | nonrel. | 7.9647 | 5.0696 | 0.0 | 2.0 |
| | rel. | 7.8358 | 5.6734 | -4.89 | 5.5 |
| W: | rel. | 7.4322 | 5.9902 | 0.0 | 2.0 |
| | rel. | 7.2098 | 7.1139 | -9.10 | 5.5 |
| W: | rel. | 8.9565 | 5.2637 | 0.0 | 3.0 |
| | rel. | 8.9104 | 5.4957 | -1.89 | 5.5 |

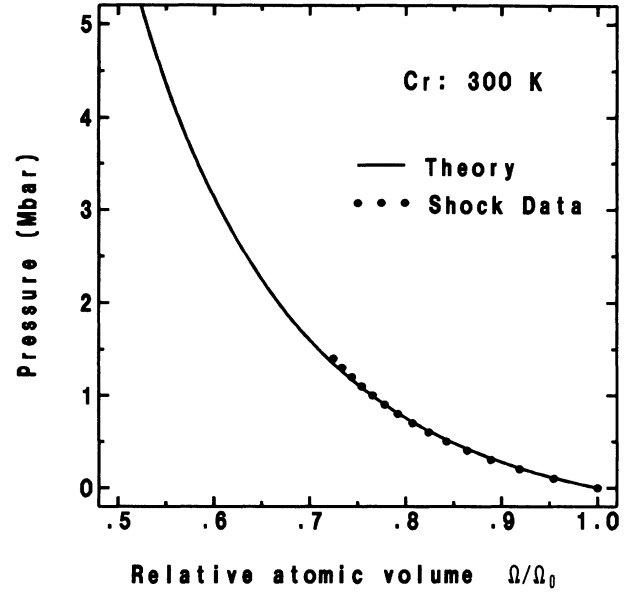


FIG. 10. Present theoretical 300-K isotherm calculated for bcc Cr compared against the shock-reduced data of Ref. 37.

where $X \equiv (\Omega/\Omega_0)^{1/3}$, $P_T = 3B_T$, and $\eta = 1.5(B'_T - 1)$. Here B_T and B'_T are the isothermal bulk modulus and its first pressure derivative, respectively, at $\Omega = \Omega_0$. In our calculational procedure, the shape of the pressure-volume relation has been unaltered by temperature, so that $B_T = B_0$ and $B'_T = B'_0$. The additional parameter β in Eq. (10) can be directly related to the second pressure derivative B''_0 . In the standard form of the universal equation of state one takes $\beta = 0$, which is both appropriate and optimum here for small values of $1 - X$. The values of B_0

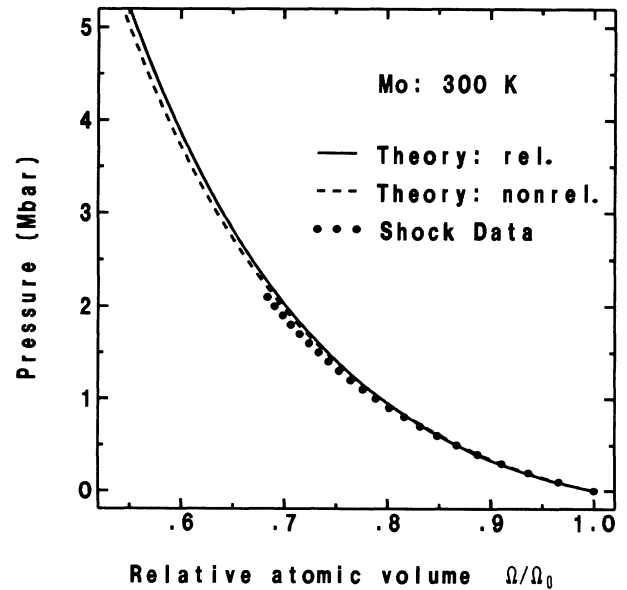


FIG. 11. Present theoretical 300-K isotherms for bcc Mo calculated from both the nonrelativistic and the scalar-relativistic treatments compared against the shock-reduced data of Ref. 37.

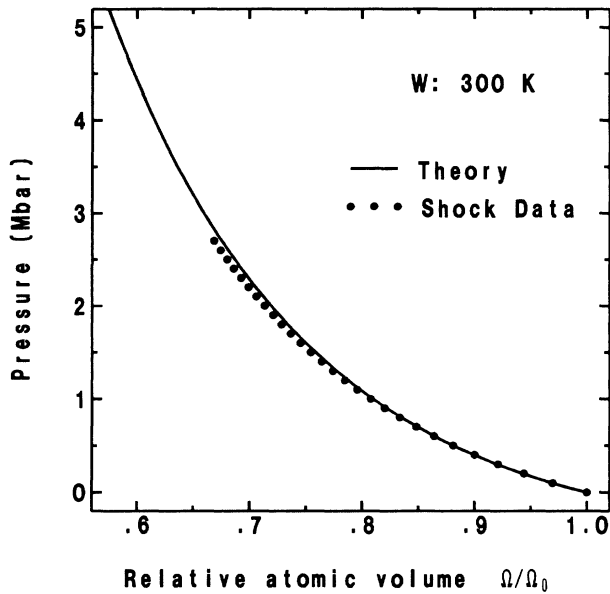


FIG. 12. Present theoretical 300-K isotherm calculated for bcc W compared against the shock-reduced data of Ref. 37.

and B'_0 we have obtained with $\beta=0$ for all three metals are compared with experiment^{35,36} in Table III. The agreement is seen to be very good, especially for Mo and W. For larger values of $1-X$ in Mo and W, however, the additional parameter β is necessary to extend Eq. (10) all the way up to the desired 5–6-Mbar pressure range. With $\beta=0$, good fits to P_{300} could be obtained for these metals only up to about 2–3 Mbar. In the case of Cr, on the other hand, allowing a nonzero value of β did not improve the overall fit below 6 Mbar, so we have maintained $\beta=0$ in this metal. A complete set of fitting parameters we have obtained in connection with Eq. (10) is given in Table IV. In deriving these parameters, LMTO data bases of 8, 9, and 6 pressure points (equally spaced in Ω/Ω_0) were used for Cr, Mo, and W, respectively. Over the pressure ranges indicated in Table IV (i.e., up to P_{\max}), these data were generally fit to an accuracy of better than 1% in the cases of Mo and W, but a somewhat lower accuracy in the case of Cr.

Our full calculated 300-K isotherms for bcc Cr, Mo, and W are compared with the shock data of McQueen *et al.*³⁷ in Figs. 10–12, respectively. This data, which extends only to the 1.5–2.5-Mbar range, has been reduced from the measured Hugoniot under conditions similar to those assumed in Eq. (9), namely, with $P_{\text{zero}}=0.0$ and $\gamma_{\text{ion}}(\Omega)/\Omega=\text{const}$ in Eq. (8) and with $P_{\text{el}}=0.0$. The overall agreement between theory and experiment is again seen to be very good, although in Mo and W theory predicts slightly stiffer isotherms above 2 Mbar than suggested by the data. Also note in the case of Mo that there is only a small difference between the nonrelativistic and scalar-relativistic results.

V. DISCUSSION AND CONCLUSIONS

It finally remains to compare and attempt to reconcile our predicted ultrahigh-pressure phase transitions in the

group-VIB elements with the existing diamond-anvil-cell (DAC) measurements^{9,10} and shock-wave data^{7,8} on these metals. In Table V we summarize all of the current theoretical and experimental results relevant to the high-pressure destabilization of the bcc structure in Cr, Mo, and W. The present theoretical analysis yields a predicted zero-temperature bcc→hcp transition in these metals at about 7.0, 4.2, and 12.5 Mbar, respectively, assuming no intermediate low-symmetry phase occurs between bcc and hcp. The room-temperature DAC studies on Mo and W have been carried out to 4.16 and 3.78 Mbar, respectively, with the bcc structure observed to remain stable in both metals. These results are then still con-

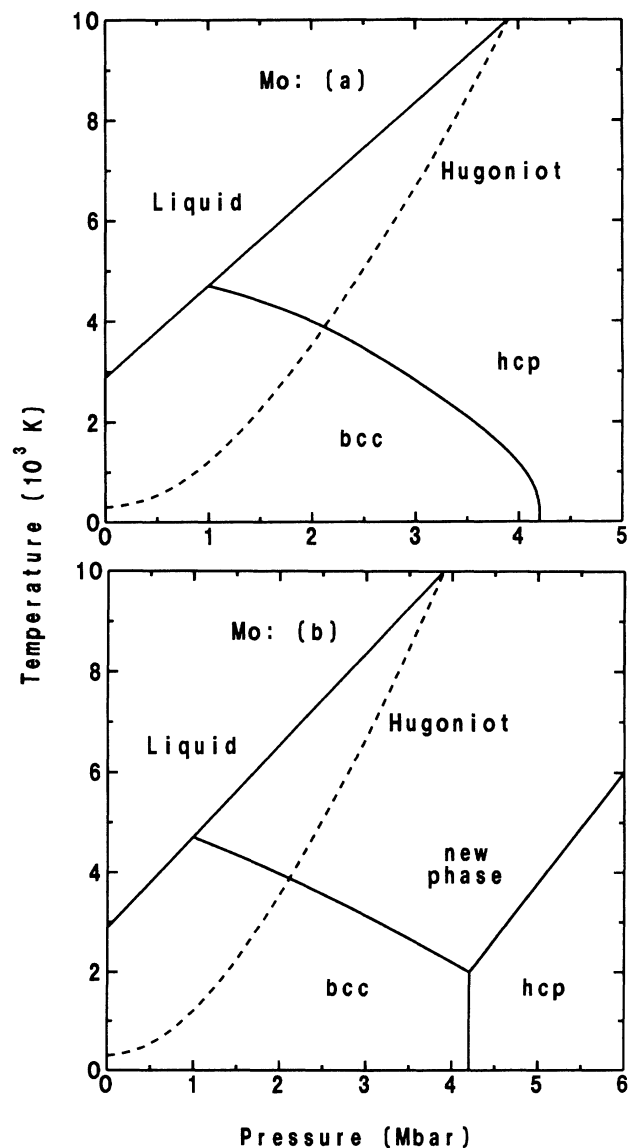


FIG. 13. Schematic representation of two possible pressure-temperature phase diagrams for Mo consistent with the present theoretical calculations and current experimental data. (a) A strongly temperature-dependent bcc-hcp phase line. (b) A new high-temperature solid phase.

TABLE V. Summary of current data on the high-pressure destabilization of the bcc structure in the group-VIB metals. Theory represents the present prediction of a bcc→hcp transition, with the corresponding transition pressures from Table II. Pressures (P) are given in Mbar and temperatures (T) are given in K.

| | Theory | | Diamond-anvil cell | | Shock compression | |
|-----|--------|-----|---------------------|-----|-------------------|---------------------|
| | P | T | P | T | P | T |
| Cr: | 7.0 | 0 | | | | |
| Mo: | 4.2 | 0 | > 4.16 ^a | 300 | 2.1 ^b | 4 000 ^d |
| W: | 12.5 | 0 | > 3.78 ^a | 300 | 4.3 ^c | 11 000 ^d |

^aReference 10.

^bReference 7.

^cReference 8.

^dPresent estimate based on the calculated Hugoniot temperature at the measured pressure.

sistent with our calculations, even though no evidence of a phase transition has yet been obtained. In the case of W, our calculations indicate that there is little immediate prospect of observing such a phase transition by further increases in DAC pressure, while in the case of Mo, on the other hand, the prospect would appear to be excellent. In the corresponding high-temperature shock-wave studies of Mo and W, evidence for the destabilization of the bcc structure through a solid-solid phase transition has been found at 2.1 and 4.3 Mbar, respectively. These transition pressures represent 50 and 35 % of our predicted zero-temperature values and clearly suggest very large high-temperature effects on the solid phase diagrams of these metals. We estimate the transition temperatures in the shock-wave experiments to be about 4000 K in Mo and 11 000 K in W. Two possible phase diagrams which could reconcile theory and experiment here are indicated schematically in Fig. 13 for the case of Mo. The first possibility [Fig. 13(a)] is for a very strong temperature dependence to the bcc-hcp phase line. Preliminary GPT calculations on Mo suggest that quasiharmonic phonons alone probably *cannot* account for such a large quantitative effect, so that either large anharmonic effects and/or large electron-thermal effects would be necessary. A large electron-thermal contribution is, in fact, expected here due to the increase in the density of states at E_F in the hcp structure over the bcc structure for a group-VIB metal.³⁸ The second possibility [Fig. 13(b)] is for an additional high-temperature solid phase, such that the shock measurements are actually detecting a transition to this phase rather than to hcp. It is unclear, however, what the nature of such a phase might be. Alloys of Mo and W with transition elements to the right of the group-VIB metals do reveal several candidate structures, but the majority of these are characteristic of compound formation and not likely to occur in the elemental metal. Two exceptions are the A15 or β -W structure which occurs in Mo-Re and Mo-Os alloys and the A12 or α -Mn structure which occurs in Mo-Re and W-Re alloys.³⁹

One further interesting experimental possibility is to attempt to lower the room-temperature bcc→hcp transition pressure by alloying bcc group-VIB metals with hcp group-VIIB or group-VIII elements. In this regard, perhaps the most interesting system for study would be the Mo-Re alloy. For this system, the bcc Mo-rich solid solution forms at high temperature for Re concentrations up to $\approx 40\%$,³⁹ so that presumably the bcc→hcp transition pressure, even if in pure Mo it is above the 4.2 Mbar we calculate, could be reduced to well within the DAC measurement range. If the bcc→hcp transition can indeed be observed in Mo or a dilute Mo-Re alloy, it would then also be of great interest to examine the temperature dependence of the phase line in an attempt to distinguish between the two hypothetical phase diagrams shown in Fig. 13.

In the future it may be possible to map out entire theoretical pressure-temperature phase diagrams for the group-VIB metals by combining LMTO and GPT calculations. The LMTO approach can be extended to finite temperature within the regime of $k_B T \ll E_F$ to examine the effects of electron-thermal contributions on the bcc-hcp phase line. The GPT approach, on the other hand, can be combined with molecular-dynamics or Monte Carlo simulation to examine the corresponding effects of ion-thermal contributions, to search for new possible high-temperature solid phases, and to investigate melting.

ACKNOWLEDGMENTS

This work was performed under the auspices of the U.S. Department of Energy by Lawrence Livermore National Laboratory under Contract No. W-7405-Eng-48. The author wishes to thank Dr. Rob Hixson for sharing his preliminary shock data on W and permission to quote these results here. The author also acknowledges helpful comments from Dr. John Shaner, Professor Wilfried Holzappel, and Professor David Pettifor.

¹R. A. Deegan, J. Phys. C **1**, 763 (1968); N. W. Dalton and R. A. Deegan, *ibid.* **2**, 2369 (1969); D. G. Pettifor, *ibid.* **3**, 367 (1970).

²J. C. Duthie and D. G. Pettifor, Phys. Rev. Lett. **38**, 564 (1977).

³E.g., H. L. Skriver, Phys. Rev. B **31**, 1909 (1985).

⁴U. Benedict, W. A. Grosshans, and W. B. Holzappel, Physica B **144**, 14 (1986).

⁵A. K. McMahan, Physica B **139&140**, 31 (1986).

- ⁶V. A. Zil'bershteyn, L. B. Zaretskiy, and E. I. Estrin, *Fiz. Metal. Metaloved.* **40**, 587 (1975).
- ⁷R. S. Hixson, D. A. Boness, J. W. Shaner, and J. A. Moriarty, *Phys. Rev. Lett.* **62**, 637 (1989).
- ⁸R. S. Hixson (private communication).
- ⁹Y. K. Vohra and A. L. Ruoff, *Phys. Rev. B* **42**, 8651 (1990).
- ¹⁰A. L. Ruoff, H. Xia, H. Luo, and Y. K. Vohra, *Rev. Sci. Instrum.* **61**, 3830 (1990).
- ¹¹J. M. Brown and J. W. Shaner, in *Shock Waves in Condensed Matter—1983*, edited by J. R. Asay, R. A. Graham, and G. K. Straub (North-Holland, Amsterdam, 1984), p. 91.
- ¹²Y. K. Vohra, S. J. Duclos, and A. L. Ruoff, *Phys. Rev. B* **36**, 9790 (1987).
- ¹³R. E. Watson, J. W. Davenport, M. Weinert, and G. Fernando, *Phys. Rev. B* **38**, 7817 (1988).
- ¹⁴H. Xia, S. J. Duclos, A. L. Ruoff, and Y. K. Vohra, *Phys. Rev. Lett.* **64**, 204 (1990).
- ¹⁵H. Xia, G. Parthasarathy, H. Luo, Y. K. Vohra, and A. L. Ruoff, *Phys. Rev. B* **42**, 6736 (1990).
- ¹⁶J. S. Gyanchandani, S. C. Gupta, S. K. Sikka, and R. Chidambaram, *High Pressure Res.* **4**, 472 (1990); *J. Phys.: Condens. Matter* **2**, 301 (1990); **2**, 6457 (1990).
- ¹⁷H. K. Mao, Y. Wu, L. C. Chen, J. F. Shu, and A. P. Jephcoat, *J. Geophys. Res.* **95**, 21 737 (1990).
- ¹⁸J. A. Moriarty, *Phys. Rev. B* **38**, 3199 (1988).
- ¹⁹N. C. Holmes, J. A. Moriarty, G. R. Gathers, and W. J. Nellis, *J. Appl. Phys.* **66**, 2962 (1989).
- ²⁰W. Kohn and L. J. Sham, *Phys. Rev.* **140**, A1133 (1965).
- ²¹O. K. Andersen, *Phys. Rev. B* **12**, 3060 (1975); O. K. Andersen and O. Jepsen, *Physica B* **91**, 317 (1977).
- ²²H. L. Skriver, *The LMTO Method* (Springer, Berlin, 1984).
- ²³L. Hedin and B. I. Lundqvist, *J. Phys. C* **4**, 2064 (1971).
- ²⁴E.g., J. A. Moriarty and A. K. McMahan, *Phys. Rev. Lett.* **48**, 809 (1982); A. K. McMahan and J. A. Moriarty, *Phys. Rev. B* **27**, 3235 (1983).
- ²⁵D. G. Pettifor, *Commun. Phys.* **1**, 141 (1976); D. A. Liberman, *Phys. Rev. B* **3**, 2081 (1971).
- ²⁶A. R. Mackintosh and O. K. Andersen, in *Electrons at the Fermi Surface*, edited by M. Springford (Cambridge University, Cambridge, 1980).
- ²⁷L. F. Mattheiss and D. R. Hamann, *Phys. Rev. B* **33**, 823 (1986).
- ²⁸C. T. Chan, D. Vanderbilt, S. G. Louie, and J. R. Chelikowsky, *Phys. Rev. B* **33**, 7941 (1986).
- ²⁹W. J. Nellis, J. A. Moriarty, A. C. Mitchell, M. Ross, R. G. Dandrea, N. W. Ashcroft, N. C. Holmes, and G. R. Gathers, *Phys. Rev. Lett.* **60**, 1414 (1988).
- ³⁰A. C. Mitchell, W. J. Nellis, J. A. Moriarty, R. A. Heinle, N. C. Holmes, R. E. Tipton, and G. W. Repp, *J. Appl. Phys.* **69**, 2981 (1991).
- ³¹J. A. Moriarty, *Phys. Rev. B* **42**, 1609 (1990).
- ³²W. B. Pearson, *Handbook of Lattice Spacings and Structures of Metals* (Pergamon, New York, 1967).
- ³³P. Vinet, J. H. Rose, J. Ferrante, and J. R. Smith, *J. Phys.: Condens. Matter* **1**, 1941 (1989); P. Vinet, J. Ferrante, J. H. Rose, and J. R. Smith, *J. Geophys. Res.* **92**, 9319 (1987).
- ³⁴S. K. Sikka, *Phys. Rev. B* **38**, 8463 (1988).
- ³⁵M. W. Finnis and J. E. Sinclair, *Philos. Mag. A* **50**, 45 (1984).
- ³⁶K. W. Katahara, M. H. Manghnani, and E. S. Fisher, *J. Phys. F* **9**, 773 (1979).
- ³⁷R. G. McQueen, S. P. Marsh, J. W. Taylor, J. M. Fritz, and W. J. Carter, in *High Velocity Impact Phenomena*, edited by R. Kinslow (Academic, New York, 1970), Chap. VII.
- ³⁸J. W. Shaner, in *Shock Compression of Condensed Matter—1989*, edited by S. C. Schmidt, J. N. Johnson, and L. W. Davison (North-Holland, Amsterdam, 1990), p. 121.
- ³⁹*Binary Alloy Phase Diagrams*, edited by T. B. Massalski (American Society for Metals, Materials Park, Ohio, 1990).

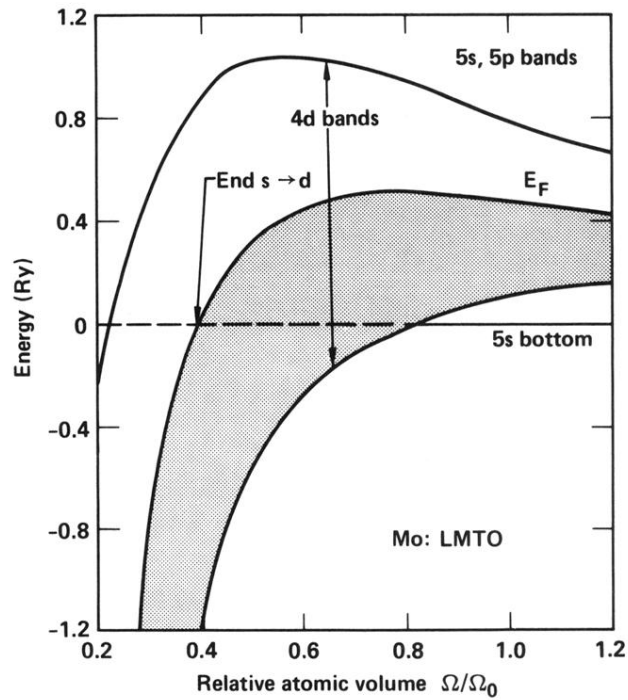


FIG. 5. Lowering of the $4d$ bands and the Fermi level E_F relative to the $5s$ and $5p$ bands with decreasing volume for nonrelativistic Mo. Nominal end to the $s \rightarrow d$ transition occurs when E_F falls below the bottom of the $5s$ band. Included in the calculation but not shown are the complicating effects of $sp-d$ hybridization and the emergence of the outer-core $4s$ and $4p$ bands from below. Occupied portion of the $4d$ bands is shaded.